Micromechanical Mechanisms for Toughness Enhancement in β-Modified Polypropylene

Sven Henning,[1] *Rameshwar Adhikari,*[1] *Georg H. Michler,**[1]
Francisco J. Baltá Calleja,[2] *József Karger-Kocsis*[3]

[1]Institute of Materials Science, Martin Luther University Halle Wittenberg, D-06099 Halle, Germany
E-mail: michler@iw.uni-halle.de
[2]Instituto de Estructura de la Materia, CSIC, Serrano 119, 28006 Madrid, Spain
[3]Institute of Composite Materials, University of Kaiserslautern, D-67633 Kaiserslautern, Germany

Summary: Two samples of isotactic polypropylene (iPP) representing the crystalline α- and β- modifications are compared with regard to their semicrystalline morphology and the resulting micromechanical mechanisms. Processes at room temperature (23°C) and at –40°C have been investigated by means of different microscopic techniques. Good results can be achieved by the application of a chemical etching technique to the deformed samples prior to scanning electron microscopy inspection. The toughness enhancement that is measured for the β-iPP is attributed to micromechanical mechanisms initiated within the intercrystalline, amorphous phase. It is shown that the specific nanostructure (lamellar arrangement) causes significant changes in the mechanical behaviour of the materials.

Keywords: deformation behaviour; electron microscopy; microhardness; nanostructure; polypropylene; semicrystalline polymers

Introduction

Isotactic polypropylene (iPP) belongs to the family of commodity plastics and occupies the third place after low-density polyethylene (LDPE) and polyvinyl chloride (PVC) in the worldwide plastic market. The most important applications of this polymer are the production of films, textile fibres and moulded parts in which the plastic is processed mainly by extrusion and injection moulding.[1, 2] The pronounced diversity of this polymeric material is also connected with the existence of several crystal modifications.[3] Of particular interest from a technical point of view is the β-modification of PP because of its enhanced toughness compared to the ordinary α-modification.[4, 5] The copolymers, blends and composites containing iPP find application in several fields of everyday life. The aim of this work is to analyze the micromechanical mechanisms responsible for the enhanced toughness of the β-iPP compared to that of common α-modification.

 DOI: 10.1002/masy.200451012

Experimental

Materials

Polypropylene samples were prepared from two high molecular weight commercial isotactic polypropylene grades (BOREALIS AG): α-iPP was Daplen BE50 and β-iPP was Daplen BE60. Sheets of a thickness of 1 mm were produced using a hot press and subsequent multistage crystallization procedure in the second β-iPP case. Miniaturized, dumbbell-shaped tensile bars were punched out of the plates using a special pierce tool.

Mechanical Testing

A MINIMAT miniature materials testing device (POLYMER LABORATORIES, UK) was used to perform tensile deformation experiments at a cross-head speed of 1 mm/min at room temperature. Stress-strain diagrams were recorded to qualitatively follow the states of deformation. They will not be discussed in detail in this work because they represent single events and the experiments do not follow any standard specification. A custom-made heating/cooling chamber adapted for the MINIMAT device was used to perform tensile experiments at –40°C. The cooling was provided by a nitrogen flow. The temperature was measured close to the sample surface by means of a digital thermocouple thermometer. Samples were elongated until fracture without recording the stress-strain-curves.

Scanning Electron Microscopy (SEM)

In order to obtain a planar geometry and flat surfaces, the deformed samples were embedded in epoxy resin and microtomed down to the middle section of the tensile bar using a LEICA microtome with a metal blade. Regions of interest corresponding to the different states of deformation were selected for SEM investigations (Fig. 1). Subsequently, a modified permanganic etching technique according to OLLEY and BASSETT [6] was applied to reveal the morphology of the deformed material. For our procedure, a mixture of 5 ml distilled water and 50 ml concentrated sulphuric acid plus 0.55 g $KMnO_4$ was adequate. We found that an etching time of 15 to 30 minutes gave optimum results. To avoid electrical charging, samples were sputter-

coated with a gold layer of 12 nm (EDWARDS sputter coater). Micrographs of the deformation structures were recorded using a JEOL JSM 6300 scanning electron microscope operated at 15 kV accelerating voltage.

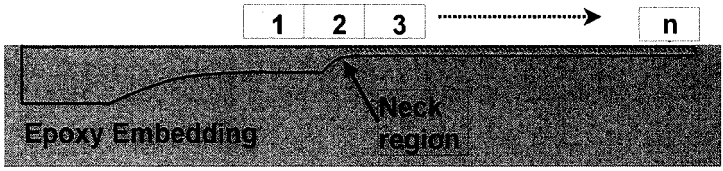

Figure 1. Outline of the preparation procedure. The embedded tensile bar is microtomed down to the middle. After chemical etching, SEM micrographs were taken at regions representing different states of deformation (1, 2, 3, ... n).

Scanning Force Microscopy (SFM)

The morphology of untreated surfaces of α- and β-iPP samples crystallized from the melt were imaged using a DIGITAL INSTRUMENTS SFM equipped with a NANOSCOPE IIIa controller. A silicon cantilever with a resonance frequency of approx. 300 kHz and a spring constant of approx. 15 N/m was used. Best results concerning the information on the semicrystalline morphology were obtained in the tapping mode. Only phase images are presented.

Transmission Electron Microscopy (TEM)

From non-deformed and from elongated samples similar to those used for SEM investigations, ultrathin sections were prepared from regions of interest close to the middle of the tensile bar. The materials were stained in RuO_4 vapour for several hours. For the preparation of the approx. 100 nm thick ultrathin sections, a LEICA ULTRACUT microtome equipped with a DIATOME diamond knife was used. Micrographs were acquired using a JEOL JSM 2010 microscope operated at 200 kV accelerating voltage.

Microhardness

In order to obtain a co-planar geometry and flat surfaces, the deformed samples were embedded

in epoxy resin and microtomed down to the middle section of the tensile bar using a LEICA microtome equipped with a metal blade. Surface effects (skin morphology or scratches) were thereby eliminated. For the microindentation experiments the regions corresponding to the different states of deformation were selected (similar to SEM preparation, Fig. 1).

Microhardness measurements were performed at room temperature using a LEITZ microhardness tester equipped with a Vickers square pyramidal diamond indenter (168°). Indentation experiments were performed using a load of 98.1 mN and a loading time of 0.1 min. The final permanent deformation was measured immediately after load release using the micrometer eyepiece of the microscope. Microindentations were performed starting from undeformed regions and proceeding in equidistant steps of 100 to 150 μm across the neck region into the cold drawn area. The hardness values expressed in [MPa] were calculated from the residual projected area of the indentation using the relation:

$$H = kP/d^2 \tag{1}$$

where d is the length [μm] of the impression diagonal, P is the load [N] applied and k is a geometrical factor equal to 1.854×10^6.[7] The hardness values were derived from the indention diagonals parallel $H_{\parallel}$ and normal $H_{\perp}$ to the straining direction. Each data point represents the average of at least four indentations.

Morphology

The most significant morphological feature of the more common α-form of the iPP is the so-called "cross-hatched" arrangement of the crystalline lamellae, as shown in Fig. 2. The main lamellae ("mother lamellae") grow radically from an initial site (centre of the spherulite), whereas the "daughter lamellae" are formed by an epitaxial growth onto them, exhibiting a typical angle of 81°[8]. In contrast to that phenomenon, a stacked, parallel arrangement of bundles of lamellae is found for the β-modified material (Figs. 2, 3). Here, the lamellae form a more sheaves-like superstructure rather than a pure radiating, spherulitic growth. From the SFM and TEM micrographs it becomes clear that the intercrystalline, amorphous portion is distributed more continuously in case of the β-iPP. In other words, the latter shows the typical lamellar structure as

it is at hand in other major semicrystalline polymers (LDPE, HDPE, UHMWPE).[9, 10]

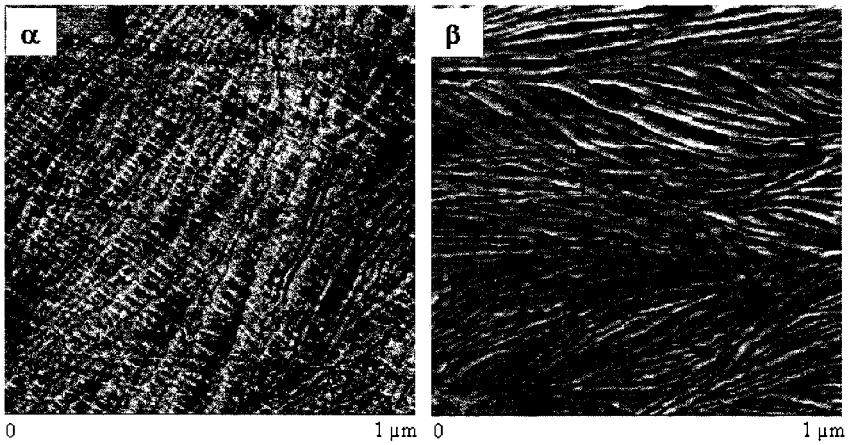

Figure 2. Comparison of the semicrystalline morphologies of α - and β- iPP. The arrangements of the crystalline lamellae (brighter shades of grey) and the amorphous portion (dark) differ significantly. Tapping mode SFM images, phase contrast.

The crystalline lamellae of the β-iPP are slightly thicker (approx. 15 nm) than the lamellae found in the α-iPP (approx. 10 nm). Due to the nucleating agent that was added by the producer in the case of the β-modified material, the size of the spherulites is different for the two materials. For the α-iPP the average diameter is approx. 50 µm, for the β-iPP the average diameter is reduced to approx. 10 µm. From the SEM micrographs we conclude that the β-modified material is "pure", since the whole area of the sample is filled with spherulitic superstructures that can be assigned to the crystalline β-modification.

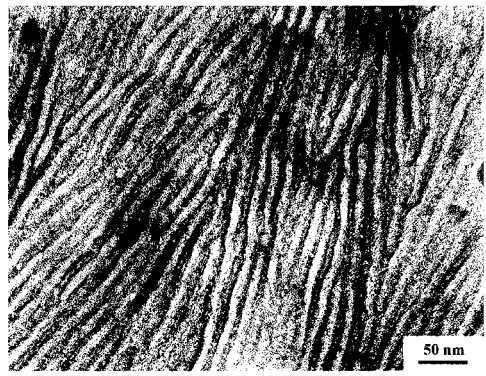

Figure 3. Stack-like arrangement of crystalline lamellae (bright) and intercrystalline, amorphous material (dark) in the β-modification of polypropylene. TEM micrograph, RuO_4 stained.

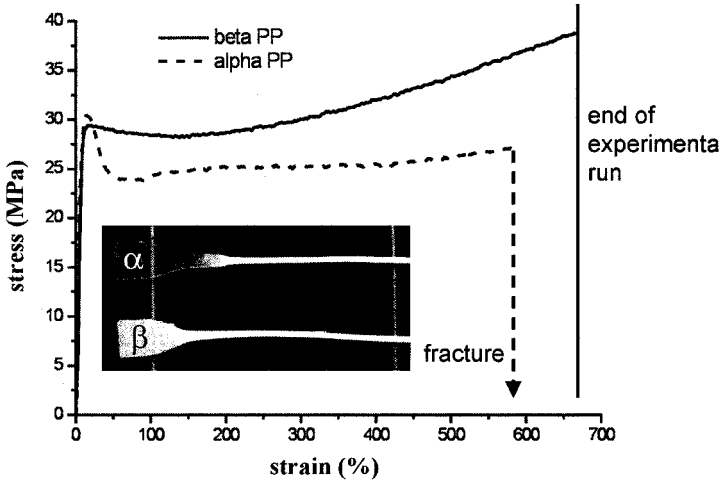

Figure 4. Comparison of the stress-strain curves obtained for miniaturized tensile bars at room temperature. Due to the geometrical limitation of the tensile device the β-iPP bar could not be drawn up to fracture.

Deformation at 23°C: Comparison of the Micromechanical Mechanisms

The plastic deformation of the tensile bars of both PP types under load proceeds via formation and propagation of two necks in opposite directions. The tensile stresses at yield are comparable (approx. 30 MPa in both cases), and the curves for the elastic part before the yield point coincide. Due to the geometrical limitations of the miniature tensile tester, the β-iPP sample was not drawn up to the fracture. The strain at break for the α-iPP sample is approx. 600 %. If we consider that the area below the stress-strain curves can be taken as a measure for the energy that is dissipated by plastic deformation within the sample, then the β-iPP is superior.

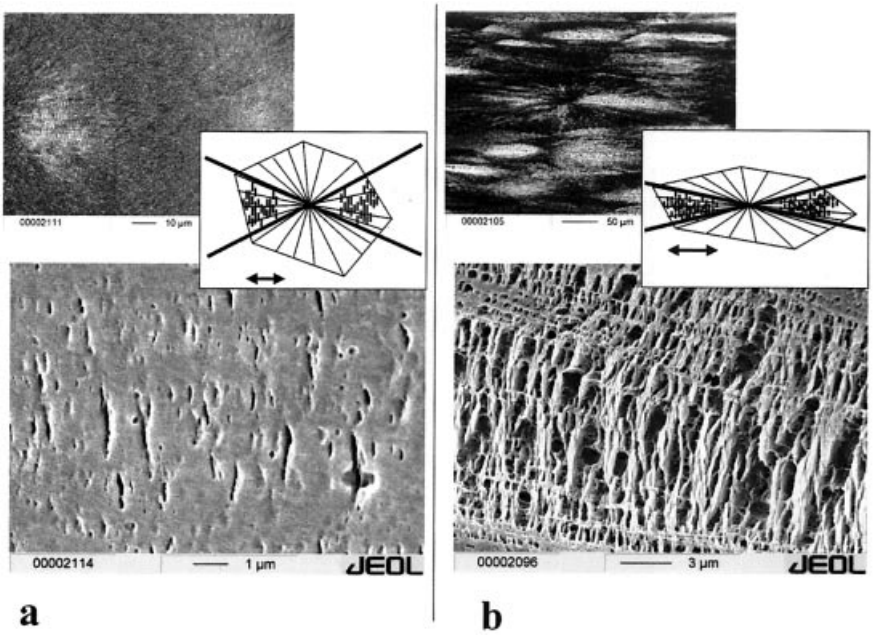

Figure 5. Micromechanical processes in α-iPP for initial stages of deformation at 23°C. The approximate elongations represented in the micrographs are $\lambda \cong 1.1$ (a) and $\lambda \cong 2$ (b), respectively. The lower images are higher magnifications from selected areas in the overview images. SEM micrographs after chemical etching.

In Fig. 5 the structural changes within the sample are shown for initial stages of deformation, i.e. for elongations up to $\lambda \cong 2$. The formation of microvoids is limited to polar regions of the

spherulites (with respect to the straining direction). At higher magnifications the craze-like nature of the deformation structures becomes visible. The formation of microvoids is coupled with the fibrillation of the material. At an elongation of $\lambda \cong 2$ the mesh-like structure of the crosshatches lamellar arrangement is still to be seen (Fig. 5b).

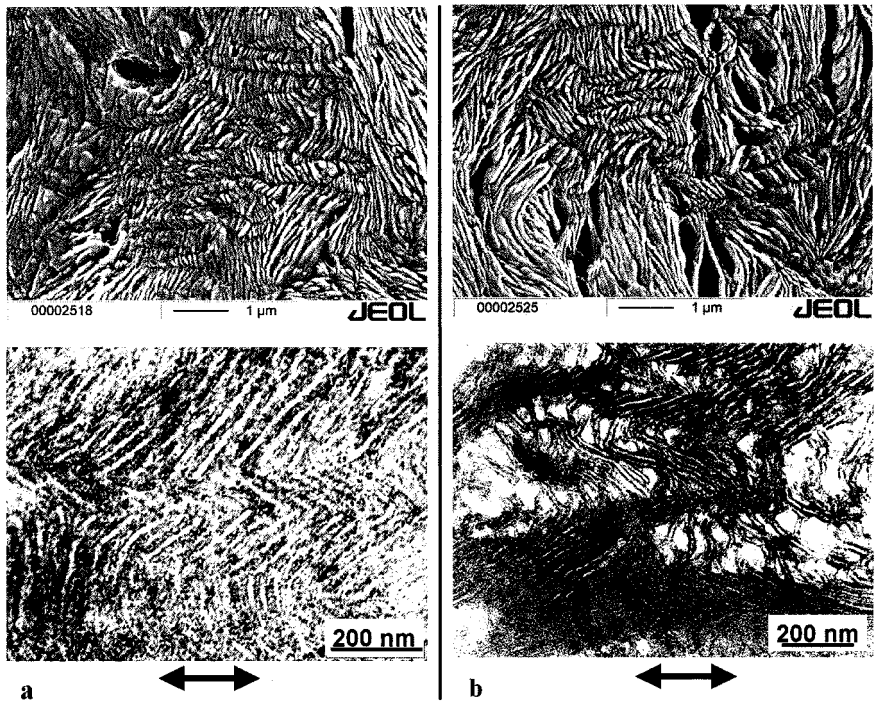

Figure 6. Micromechanical processes in β-iPP for initial stages of deformation at 23°C. The approximate elongations represented in the micrographs are $\lambda \cong 1.2$ (a) and $\lambda \cong 1.4$ (b), respectively. The upper images are SEM micrographs after chemical etching and the lower ones are TEM results obtained for similar regions (RuO_4 stained).

In contrast to the results for the α-iPP, the whole sample area contributes to micromechanical processes that are connected with microvoid formation and fibrillation. We have found no dependency of the intensity of microvoiding from the actual situation of the investigated area with respect to the straining direction. In Fig. 6 the structures observed at elongations of $\lambda \cong$

1.2(a) and $\lambda \cong 1.4$ (b), respectively, are given. In this case the orientation of the lamellae was perpendicular to the straining direction. Two general processes are observed concurrently: the formation of a so-called "chevron"-pattern and lamellar separation. The first process can be interpreted as a collective twisting of bundles of lamellae. There is neither microvoid formation nor fibrillation. The most interesting aspect is that similar processes are observed for other materials with lamellar morphologies, as there are other semicrystalline polymers (such as polyethylenes [9, 10]) and styrene/butadiene block copolymers[11]. The second process includes the formation of microvoids and fibrillation. Lamellar separation is dominated by the deformation of the intercrystalline, amorphous material (Fig. 9). The actual nanostructure, i.e., the lamellar arrangement of a hard (crystalline) and a soft (amorphous) phase connected by entangling as well as tie molecules dominates the deformation process. Structural features in the range of 10 nm initiate craze-like deformation processes. These crazes are highly localized zones of plastic deformation, but the small size and the large number make that a great part of the material contributes to deformation.

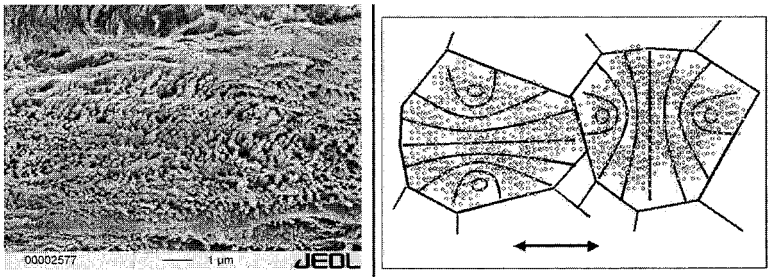

Figure 7. Micromechanical processes in β-iPP for initial stages of deformation at 23°C (REM, chemical etching). The approximate elongation λ represented in the micrograph is approx. 2 (a). The sketch in (b) indicates that, independent of the orientation of the lamellae with respect to the straining direction, intensive microvoid formation takes place in the whole volume of the material.

In Fig. 7 the crystalline lamellae are aligned parallel to the straining direction. It is observed that the lamellae are broken in fragments. Once more, intensive microvoid formation takes place. The different micromechanical mechanisms that are observed for initial stages of deformation at 23°C are outlined in Fig. 8.

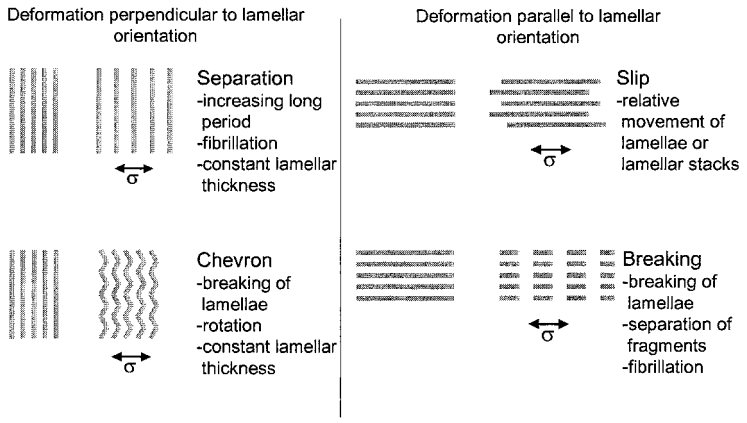

Figure 8. Comparison of different micromechanical processes induced by the lamellar morphology of the β-iPP at initial stages of deformation depending on the loading direction relative to the lamellar orientation. To some extent they are competing processes (chevron formation and lamellar separation), to some extent successive (slip before breaking).

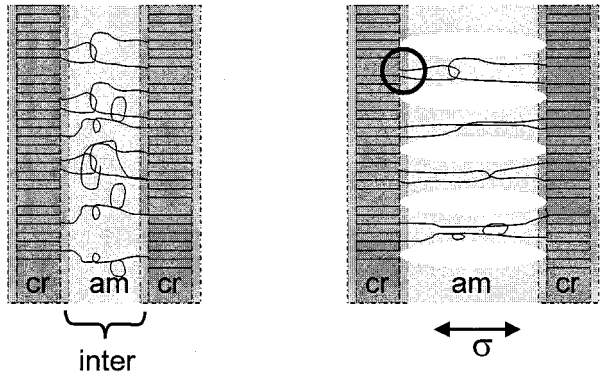

Figure 9. Illustration of the process of lamellar separation. The intercrystalline, amorphous portion is fibrillated, and nanoscopic voids are formed. For the initial deformation stage depicted here the crystalline lamellae seem to stay intact. The situation can be interpreted as a craze that is initiated by the actual semicrystalline nanostructure.

Microhardness

Starting from initial hardness values of 110 MPa for the α-iPP and 100 MPa for the β-iPP there is a significant drop as the stress whitening region or neck region is crossed. At elongations of $\lambda \cong 2$ there is a minimum in the microhardness. From the comparison of SEM images representing similar states of deformation we conclude that the drop in the microhardness is mainly caused by the intensive microvoid formation that is observed. As the deformation proceeds, an indentation anisotropy occurs, and the hardness values increase is phenomenon can be attributed to the onset of strain hardening and orientation of the material, and will be discussed elsewhere.[12]

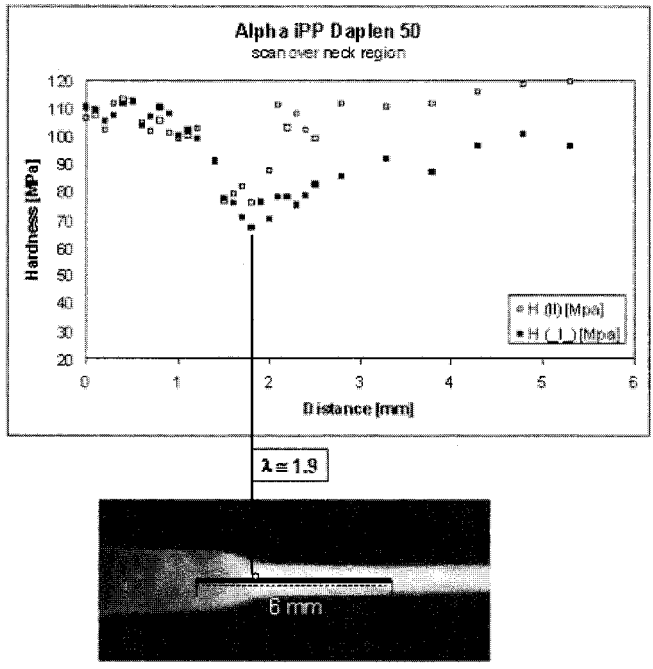

Figure 10. Changes of the microhardness (H) of α-iPP with the progression of deformation (23°C). The H values decreases significantly from an initial value of approx. 110 MPa to a minimum of approx. 70 MPa as the neck region (beginning of stress whitening) is crossed.

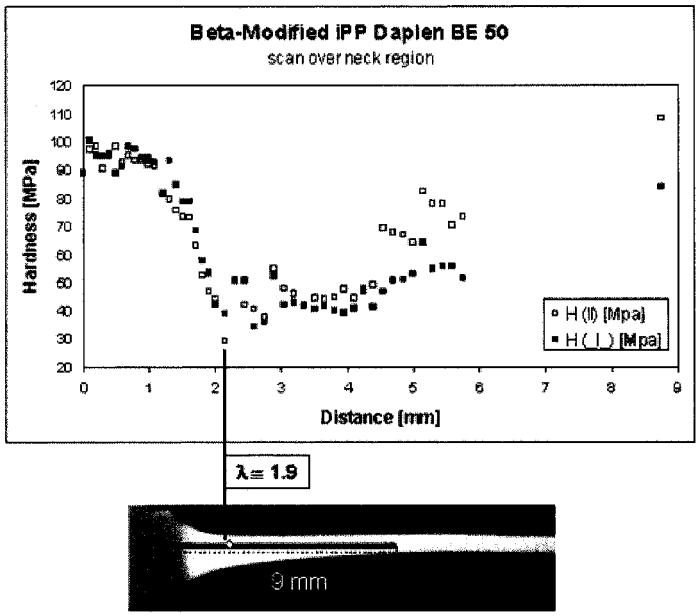

Figure 11. Changes of the Microhardness (H) of β-iPP with the progression of deformation (23°C). The magnitude of H decreases dramatically from an initial value of approx. 100 MPa to a minimum of approx. 35 MPa on going through the neck region (beginning of stress whitening).

Although the hardness curves for both the materials examined are similar, the drop in hardness that is observed for the β-modification is much greater (Fig. 11). This observation correlates well with the micromechanical processes connected with intensive microvoid formation for the β-iPP. This is in good agreement with the SEM results, showing that more sample volume contributes to microvoiding in the case of the β-iPP.

Deformation at -40°C: Comparison of the Micromechanical Mechanisms

At temperatures below the glass transition temperature (T_g) of the amorphous phase (approx. 0°C) polypropylene tends to become brittle. Toughness enhancement measures also have overcome the problems related to low temperature applications.

For both of the systems investigated, the material becomes brittle when tested at –40°C. Typical crazes are observed. The crazes are not influenced by the spherulitic morphology; they run perpendicular to the straining direction, and the edges are bridged by fibrils (Fig. 12). The crazes in the β-modified PP are finer and shorter, and there are much more to be seen in a similar sample area. That means that even at low temperatures more plastic deformation can take place as crazing is the major energy dissipating process. The multiple crazing should result in a tougher material. Nevertheless, none of the nanostructure-controlled processes discussed earlier were found in the samples deformed at –40°C. These nanomechanical processes are initiated by the more mobile amorphous material, and they are freezing as the loading temperature is below the T_g of the amorphous phase.

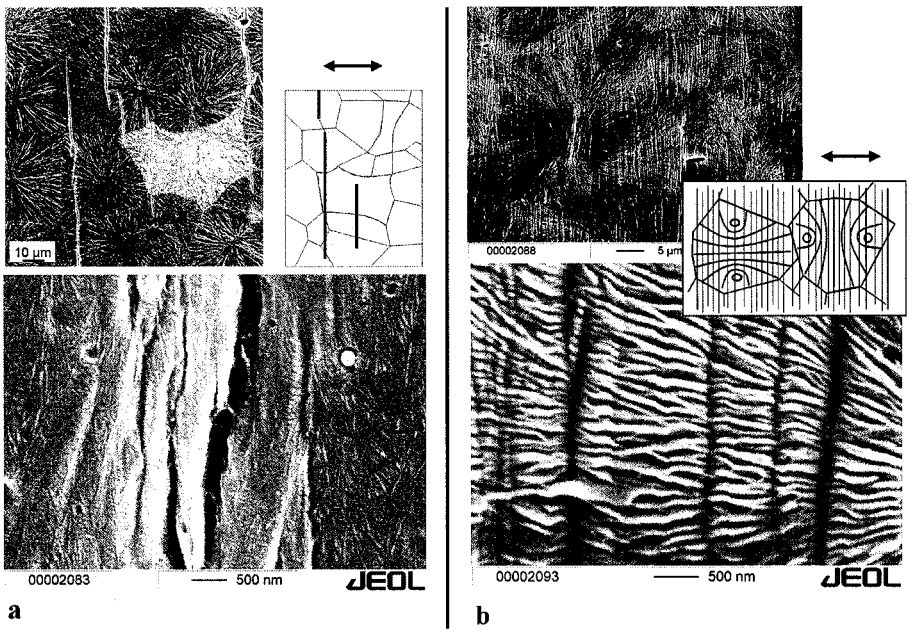

Figure 12. Comparison of the micromechanical mechanisms observed at –40°C. Only few, but long and coarse, crazes are typical for the α-modification (a). Fibrillation is clearly to be seen (a, lower image). The crazes generated in the β-iPP are smaller and thinner (b). Due to a large number of crazes, more material contributes to plastic deformation. SEM after chemical etching.

Conclusions

Although there is a number of publications on the deformation behaviour of β-iPP[13-20] the direct comparison of the two types of polypropylene that is presented here leads to new aspects to clarify the reasons for the different mechanical properties.

Room Temperature (23°C)

For initial stages of deformation ($\lambda \leq 2$), micromechanical processes initiated by the intercrystalline, amorphous material are dominant. The enhanced toughness of the β-iPP can be explained to a great extent by the general differences in the micromechanical mechanisms that are observed by SEM and TEM. The special arrangement of the crystalline lamellae, i.e., the lamellar nanostructure of the β-modified PP, activates processes of plastic deformation that are highly localized on the nanoscale, but huge in number. They are homogeneously distributed within the volume of the stressed sample. The general processes are:

-lamellar separation with craze-like microvoid formation and fibrillation

-chevron formation

-lamellar slip

-breaking of lamellae with microvoid formation.

Sub-T_g Temperature (-40°C)

Below the T_g of the amorphous phase the intensive micromechanical processes that are responsible for the superior mechanical properties of β-iPP are freezing. Instead of the nanostructure-controlled micromechanisms, ordinary crazing takes place that can be attributed to a brittle behaviour. Nevertheless, there are many more crazes detected within the β-modification, which are thinner and shorter than that in the α-iPP. More investigations are in progress to clarify the role of this multiple crazing effect in β-iPP for toughness enhancement at low temperatures.

[1] H.G. Karian (Ed.), *"Handbook of polypropylene and polypropylene composites"*, Marcel Dekker, New York 1999.
[2] J. Karger-Kocsis (Ed.), *"Polypropylene: structure, blends and composites"*, Vol. 1. Structure and morphology, Chapman & Hall, London 1995.
[3] A. Turner Jones, J. M. Aizlewood, D. R. Beckett, *Makromol. Chem.* **1964**, *75*, 134.
[4] C. Grein, C. J. G. Plummer, H. H. Kausch, Y. Germain, P. Béguelin, *Polymer* **2002**, *43*, 3279.
[5] H. B. Chen, J. Karger-Kocsis, J. S. Wu, J. Varga, *Polymer* **2002**, *43*, 6505.
[6] R. Olley, D. C. Bassett, P. J. Hine, I. M. Ward, *J. Mat. Sci.* **1993**, *28*, 1107.
[7] F. J. Baltá Calleja, S. Fakirov, *"Microhardness of Polymers"*, Cambridge University Press, Cambridge 2000.
[8] R. A. Phillips, M. D. Wolkowitcz, in: *"Polypropylene Handbook"*, Edward P. Moore, Jr., Ed., Carl Hanser Verlag, Munich 1996, p. 113ff.
[9] G. H. Michler, K. Morawietz, *Acta Polymerica* **1991**, *42*, 620.
[10] G. H. Michler, *"Kunststoff-Mikromechanik: Morphologie, Deformations- und Bruchmechanismen von Polymerwerkstoffen"*, Carl Hanser Verlag München 1992, p. 212ff.
[11] R. Adhikari, G. H. Michler, T. A. Huy, E. Ivan´kova, R. Godehardt, W. Lebek, K. Knoll, *Macromol. Chem. Phys.* **2003**, *204*, 488.
[12] S. Henning, G. H. Michler, F. Ania, F. Baltá Calleja, *J. Coll. Polym. Sci*, submitted.
[13] P. T. S. Dijkstra, D. J. van Dijk, J. Huétink, *Polym. Eng. Sci.* **2002**, *42*, 152.
[14] M. Aboulfaraj, C. G´Sell, B. Ulrich, A. Dahoun, *Polymer* **1995**, *36*, 731.
[15] J. X. Li, W. L. Cheung, *Polymer* **1998**, *39*, 6935.
[16] J. X. Li, W. L. Cheung, C. M. Chan, *Polymer* **1999**, *40*, 2089.
[17] J. X. Li, W. L. Cheung, C. M. Chan, *Polymer* **1999**, *40*, 3641.
[18] F. Chu, T. Yamaoka, H. Ide, Y. Kimura, *Polymer* **1994**, *35*, 3442.
[19] F. Chu, T. Yamaoka, Y. Kimura, *Polymer* **1995**, *36*, 2523.
[20] T. Yoshida, Y. Fujiwara, T. Asano, *Polymer* **1983**, *24*, 925.